219

Application of aerospace structural models to marine engineering

A. Pagani*, E. Carrera[a] and R. Jamshed[b]

MUL2 Group, Department of Mechanical and Aerospace Engineering, Politecnico di Torino, Corso Duca degli Abruzzi 24, 10129 Torino, Italy

Abstract.   The large container ships and fast patrol boats are complex marine structures. Therefore, their global mechanical behaviour has long been modeled mostly by refined beam theories. Important issues of cross section warping and bending-torsion coupling have been addressed by introducing special functions in these theories with inherent assumptions and thus compromising their robustness. The 3D solid Finite Element (FE) models, on the other hand, are accurate enough but pose high computational cost. In this work, different marine vessel structures have been analysed using the well-known Carrera Unified Formulation (CUF). According to CUF, the governing equations (and consequently the finite element arrays) are written in terms of fundamental nuclei that do not depend on the problem characteristics and the approximation order. Thus, refined models can be developed in an automatic manner. In the present work, a particular class of 1D CUF models that was initially devised for the analysis of aircraft structures has been employed for the analysis of marine structures. This class, which was called Component-Wise (CW), allows one to model complex 3D features, such as inclined hull walls, floors and girders in the form of components. Realistic ship geometries were used to demonstrate the efficacy of the CUF approach. With the same level of accuracy achieved, 1D CUF beam elements require far less number of Degrees of Freedom (DoFs) compared to a 3D solid FE solution.

Keywords: hull structures; refined beam theories; unified formulation; component-wise models

1. Introduction

Nowadays, marine structures such as container ships and fast patrol boats have considerably complex structural geometries. Commonly, their structural analysis requires modeling of complete hull in a commercial Finite Element (FE) Code which may be computationally heavy. Typical ship structures such as container ships have large deck-openings for cargo area spanning over a considerable portion of their length. Considering them as a beam, their cross section resembles that of a thin-walled C-Channel. For such structures, the shear center and the area centroid of the cross section do

---

*Corresponding author, Research Assistant, E-mail: alfonso.pagani@polito.it
[a]Professor, E-mail: erasmo.carrera@polito.it
[b]Ph.D. Student, E-mail: rehan.rehan@polito.it

not coincide and a coupling between bending and torsion is observed. The structure twists when a loading force vector does not pass through shear center. Such loading scenario appears when there is an imbalance in transversely acting forces in a seaway. The twist of the beam is accompanied by out-of-plane warping (axial deformation) of the cross section at free ends. Ships have closed sections near the ends and they are relatively stiffer due to the presence of engine room at rear, the fore end or other transverse deck beams. Thus the axial displacement of a point on cross section is constrained and axial stresses (i.e., warping stresses) are generated.

The detailed and accurate deformed configuration warrants the use of commercial FE codes employing 3D solid elements. However, owing to the possible antisymmetries associated with marine structures such as torsional loading, entire ship has to be modelled and the analysis thus becomes computationally expensive. Therefore, considerable effort has been made to develop refined 1D models that are computationally lighter and can capture warping kinematics and associated stresses, see for example (Pittaluga 1978, Pedersen 1983, 1985, 1991, Senjanovic and Grubusic 1991). These beam models entail the assumption that, in addition to twisting, cross sections warp out of plane but in a rigid manner implying the presence of axial deformation only. The net warping over the whole cross section is zero meaning no net elongation of the beam.

This paper presents the structural (static and vibration) analyses of different marine vessels using refined beam model which is based on a novel approach, namely the Carrera Unified Formulation (CUF) (Carrera *et al.* 2010, 2011, 2014, Carrera and Giunta 2010). CUF provides a tool able to capture detailed kinematics of cross-section displacement field utilizing simple, refined 1D beam elements. Recently, Carrera *et al.* (2015, 2016) demonstrated CUF to effectively model various boat-like structures thereby establishing its advantage over a 3D solid FEM solution from a commercial software. The present work utilises Component-Wise (CW) models, that were initially devoted to the analysis of aerospace structures (Carrera *et al.* 2013a, b). In the CW approach, the structural features such as hull walls, transverse ribs and stiffeners are modelled as components. All components are subsequently modelled as beams with their lengths aligned to a common global axis. Interestingly, the CW approach allows to model walls as beams with the axis laying along the thickness direction. Most of the early works to model global structural behaviour of ships utilised the famous Euler-Bernoulli Beam Model (Euler 1744) (hereinafter referred to as EBBM) and Timoshenko Beam Model (Timoshenko 1922a, b) (hereinafter referred to as TBM). The EBBM imposes the condition that the plane cross sections of a beam remains plane during bending which is valid only for the cases of simple, solid and homogenous sections or long beams. EBBM ignores the transverse shear stresses that become pronounced in short beams. TBM has an additional degree of freedom that removes the perpendicularity condition of cross section from beam axis but it keeps plane cross sections as plane. However, in TBM we have constant shear stress distribution over beam cross section instead of homogenous condition at free edges and, thus, it requires a correction factor. Both EBBM and TBM do not address torsion which is modelled using Saint Venant's or Vlasov theories. For thin-walled open sections, Saint Venant's model gives only shear stresses over the cross section and not the normal warping stresses. Vlasov beam theory (Vlasov 1961) accounts for both the stresses. Leibowitz (1961) and Jensen and Madsen (1977) idealised ships as beams for hull vibrations at lower natural frequencies. The works by Bishop and Price (1974, 1975, 1979) are considered pioneering whereby two-dimensional hydroelasticity theories were established to determine structural behaviour of ship structure. The cross-section warping was addressed in works by Kawai (1973) and Senjanovic and
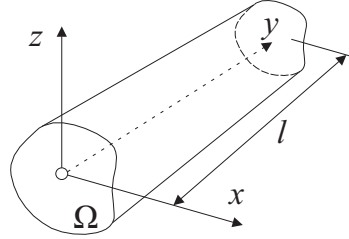
Fig. 1 Beam aligned with Cartesian coordinates

Fann (1992). In (Senjanovic and Fann 1992) a higher-order theory is developed for thin walled channel idealization for container ships. Senjanovic in his several works implemented advanced beam model while idealising ships as beam for hydroelastic analyses.

2. Carrera Unified Formulation (CUF)

According to Carrera Unified Formulation (CUF), the 3D displacement field **u** is defined in terms of generic cross-section functions F_τ

$$\mathbf{u}(x,y,z) = F_\tau(x,z)\mathbf{u}_\tau(y), \qquad \tau = 1, 2, ..., M \qquad (1)$$

where F_τ are the functions in terms of coordinates x and z over the cross-section as shown in Fig.1; M is the number of expansion terms in F_τ; and $\mathbf{u}_\tau$ is the vector of the generalized displacements. The repeated subscript, τ, indicates summation. In general, axiomatic theories of structures are defined by truncating Eq. (1) to a given order. By using CUF, the theory order is a free parameter of the formulation. Thus, the accuracy of the model can be increased with ease in order to address higher-order phenomena and surpass the limits of classic theories.

Generally, CUF allows the beam kinematics to be be approximated via different classes of expansion functions F_τ. In the present work, Lagrange Expansion (LE) polynomials (Carrera and Petrolo 2012, Carrera and Pagani 2014) have been used as cross-sectional polynomials. LE allows one to use only pure displacement variables as degrees of freedom (DoFs). An arbitrary shaped cross section is considered divided into a lattice of $iso-parametric$ Lagrange polynomials that can be 3 noded (L3), 4 noded (L4) or 9 noded (L9). The interpolation functions for one single L9 polynomial, for example, are given in Eq. (2)

$$F_\tau = \frac{1}{4}(\alpha^2 + \alpha\alpha_\tau)(\beta^2 + \beta\beta_\tau), \qquad \tau = 1, 3, 5, 7$$

$$F_\tau = \frac{1}{2}{\beta_\tau}^2(\beta^2 + \beta\beta_\tau)(1 - \alpha^2) + \frac{1}{2}{\alpha_\tau}^2(\alpha^2 + \alpha\alpha_\tau)(1 - \beta^2), \quad \tau = 2, 4, 6, 8 \qquad (2)$$

$$F_\tau = (1 - \alpha^2)(1 - \beta^2), \qquad \tau = 9$$

where α and β vary from -1 to +1, whereas α_τ and β_τ are the coordinates of the nine points whose numbering and location in the natural coordinate frame are shown in Fig. 2. The beam model resulting
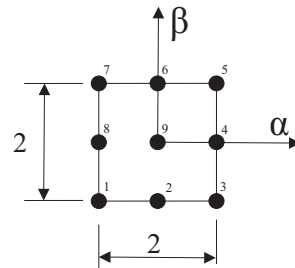
Fig. 2 L9 polynomial in natural coordinates

from the adoption of one single L9 polynomial expansion of the primary variables is given in the following

$$
\begin{aligned}
u_x &= F_1 u_{x_1} + F_2 u_{x_2} + F_3 u_{x_3} + F_4 u_{x_4} + F_5 u_{x_5} + F_6 u_{x_6} + F_7 u_{x_7} + F_8 u_{x_8} + F_9 u_{x_9} \\
u_y &= F_1 u_{y_1} + F_2 u_{y_2} + F_3 u_{y_3} + F_4 u_{y_4} + F_5 u_{y_5} + F_6 u_{y_6} + F_7 u_{y_7} + F_8 u_{y_8} + F_9 u_{y_9} \\
u_z &= F_1 u_{z_1} + F_2 u_{z_2} + F_3 u_{z_3} + F_4 u_{z_4} + F_5 u_{z_5} + F_6 u_{z_6} + F_7 u_{z_7} + F_8 u_{z_8} + F_9 u_{z_9}
\end{aligned}
\tag{3}
$$

3. Finite element formulation

3.1 Preliminaries

The coordinate system used in the present beam model is shown in Fig. 1. The beam length is l and the cross section area is Ω. The stress $\boldsymbol{\sigma}$ and strain $\boldsymbol{\epsilon}$ vectors may be written as follows

$$
\boldsymbol{\sigma} = \left\{ \begin{array}{cccccc} \sigma_{yy} & \sigma_{xx} & \sigma_{zz} & \sigma_{xz} & \sigma_{yz} & \sigma_{xy} \end{array} \right\}^T, \boldsymbol{\epsilon} = \left\{ \begin{array}{cccccc} \epsilon_{yy} & \epsilon_{xx} & \epsilon_{zz} & \epsilon_{xz} & \epsilon_{yz} & \epsilon_{xy} \end{array} \right\}^T \tag{4}
$$

The linear strain-displacement relation for small displacements and deformations is given as

$$
\boldsymbol{\epsilon} = \mathbf{D}\mathbf{u} \tag{5}
$$

where $\mathbf{D}$ is the linear differential operator on $\mathbf{u}$ and it is given as follows

$$
\mathbf{D} = \begin{bmatrix} 0 & \dfrac{\partial}{\partial y} & 0 \\[2mm] \dfrac{\partial}{\partial x} & 0 & 0 \\[2mm] 0 & 0 & \dfrac{\partial}{\partial z} \\[2mm] \dfrac{\partial}{\partial z} & 0 & \dfrac{\partial}{\partial x} \\[2mm] 0 & \dfrac{\partial}{\partial z} & \dfrac{\partial}{\partial y} \\[2mm] \dfrac{\partial}{\partial y} & \dfrac{\partial}{\partial x} & 0 \end{bmatrix} \tag{6}
$$

The constitutive law relates stress to strain through the following relation

$$
\boldsymbol{\sigma} = \mathbf{C}\boldsymbol{\epsilon} \tag{7}
$$

where $\mathbf{C}$ is the stiffness matrix. In the case of isotropic material, the terms of stiffness matrix are given in the following

$$
\mathbf{C} = \begin{bmatrix}
C_{33} & C_{23} & C_{13} & 0 & 0 & 0 \\
C_{23} & C_{22} & C_{12} & 0 & 0 & 0 \\
C_{13} & C_{12} & C_{11} & 0 & 0 & 0 \\
0 & 0 & 0 & C_{44} & 0 & 0 \\
0 & 0 & 0 & 0 & C_{55} & 0 \\
0 & 0 & 0 & 0 & 0 & C_{66}
\end{bmatrix}
\tag{8}
$$

where

$$
\begin{aligned}
C_{11} &= C_{22} = C_{33} = \frac{(1-\nu)E}{(1+\nu)(1-2\nu)} = \lambda + 2\mu \\
C_{12} &= C_{13} = C_{23} = \frac{\nu E}{(1+\nu)(1-2\nu)} = \lambda \\
C_{44} &= C_{55} = C_{66} = \frac{E}{2(1+\nu)} = G
\end{aligned}
\tag{9}
$$

In the above relations, λ and μ are the Lamé's parameters and ν, E and G are respectively the poisson's ratio, young's modulus and the shear modulus for the material.

3.2 Fundamental Nuclei

The beam is divided into finite elements with their length aligned to y-axis. By interpolating the generalized displacements $\mathbf{u}_\tau$ via shape functions N_i, Eq. (1) becomes

$$
\mathbf{u}(x, y, z) = F_\tau(x, z)N_i(y)\mathbf{q}_{\tau i}
\tag{10}
$$

where $\mathbf{q}_{\tau i}$ is the vector of the nodal generalized unknowns

$$
\mathbf{q}_{\tau i} = \left\{ \begin{matrix} q_{x_{\tau i}} & q_{y_{\tau i}} & q_{z_{\tau i}} \end{matrix} \right\}^T
\tag{11}
$$

The shape functions N_i and can be found in many standard text books about finite element method, see for example (Bathe 1996). The expansion functions F_τ for the cross-sectional kinematics and the shape function N_i are mutually completely independent. In the present work, three noded (B3) and four noded (B4) beam elements were used with quadratic and cubic approximation functions along y-axis, respectively.

In an undamped free vibration analysis, stiffness and mass matrices are required and they are obtained by employing the principle of virtual work

$$
\delta L_{\text{int}} = \int_V \delta \boldsymbol{\epsilon}^T \boldsymbol{\sigma} \, \mathrm{d}V = -\delta L_{\text{ine}}
\tag{12}
$$

where L_{int} stands for the *internal* strain energy and L_{ine} is the work done by the *inertial* loading. δ stands for the virtual variation. The virtual variation of the strain energy is rewritten using Eqs. (5), (7) and (10) as follows

$$
\delta L_{\text{int}} = \delta \mathbf{q}_{\tau i}^T \mathbf{K}^{ij\tau s} \mathbf{q}_{sj}
\tag{13}
$$

where $\mathbf{K}^{ij\tau s}$ is the *Fundamental Nucleus* (FN) of the element stiffness matrix. The nine components of the FN are mentioned below for the sake of completeness

$$
\begin{aligned}
K_{11}^{ij\tau s} &= (\lambda + 2G) \int_\Omega F_{\tau,x} F_{s,x} \mathrm{d}\Omega \int_l N_i N_j \mathrm{d}y + G \int_\Omega F_{\tau,z} F_{s,z} \mathrm{d}\Omega \int_l N_i N_j \mathrm{d}y + \\
&\quad G \int_\Omega F_\tau F_s \mathrm{d}\Omega \int_l N_{i,y} N_{j,y} \mathrm{d}y \\[2mm]
K_{12}^{ij\tau s} &= \lambda \int_\Omega F_{\tau,x} F_s \mathrm{d}\Omega \int_l N_i N_{j,y} \mathrm{d}y + G \int_\Omega F_\tau F_{s,x} \mathrm{d}\Omega \int_l N_{i,y} N_j \mathrm{d}y \\[2mm]
K_{13}^{ij\tau s} &= \lambda \int_\Omega F_{\tau,x} F_{s,z} \mathrm{d}\Omega \int_l N_i N_j \mathrm{d}y + G \int_\Omega F_{\tau,z} F_{s,x} \mathrm{d}\Omega \int_l N_i N_j \mathrm{d}y \\[2mm]
K_{21}^{ij\tau s} &= \lambda \int_\Omega F_\tau F_{s,x} \mathrm{d}\Omega \int_l N_{i,y} N_j \mathrm{d}y + G \int_\Omega F_{\tau,x} F_s \mathrm{d}\Omega \int_l N_i N_{j,y} \mathrm{d}y \\[2mm]
K_{22}^{ij\tau s} &= G \int_\Omega F_{\tau,z} F_{s,z} \mathrm{d}\Omega \int_l N_i N_j \mathrm{d}y + G \int_\Omega F_{\tau,x} F_{s,x} \mathrm{d}\Omega \int_l N_i N_j \mathrm{d}y + \\
&\quad (\lambda + 2G) \int_\Omega F_\tau F_s \mathrm{d}\Omega \int_l N_{i,y} N_{j,y} \mathrm{d}y \\[2mm]
K_{23}^{ij\tau s} &= \lambda \int_\Omega F_\tau F_{s,z} \mathrm{d}\Omega \int_l N_{i,y} N_j \mathrm{d}y + G \int_\Omega F_{\tau,z} F_s \mathrm{d}\Omega \int_l N_i N_{j,y} \mathrm{d}y \\[2mm]
K_{31}^{ij\tau s} &= \lambda \int_\Omega F_{\tau,z} F_{s,x} \mathrm{d}\Omega \int_l N_i N_j \mathrm{d}y + G \int_\Omega F_{\tau,x} F_{s,z} \mathrm{d}\Omega \int_l N_i N_j \mathrm{d}y \\[2mm]
K_{32}^{ij\tau s} &= \lambda \int_\Omega F_{\tau,z} F_s \mathrm{d}\Omega \int_l N_i N_{j,y} \mathrm{d}y + G \int_\Omega F_\tau F_{s,z} \mathrm{d}\Omega \int_l N_{i,y} N_j \mathrm{d}y \\[2mm]
K_{33}^{ij\tau s} &= (\lambda + 2G) \int_\Omega F_{\tau,z} F_{s,z} \mathrm{d}\Omega \int_l N_i N_j \mathrm{d}y + G \int_\Omega F_{\tau,x} F_{s,x} \mathrm{d}\Omega \int_l N_i N_j \mathrm{d}y + \\
&\quad G \int_\Omega F_\tau F_s \mathrm{d}\Omega \int_l N_{i,y} N_{j,y} \mathrm{d}y
\end{aligned}
\tag{14}
$$

The virtual variation of the work of the inertial loadings is

$$
\delta L_{\mathrm{ine}} = \int_V \rho \delta \mathbf{u}^T \ddot{\mathbf{u}} \mathrm{d}V
\tag{15}
$$

where ρ is the material density and $\ddot{\mathbf{u}}$ is the acceleration vector. Rewriting Eq. (15) using Eq. (10) we have

$$
\delta L_{\mathrm{ine}} = \delta \mathbf{q}_{\tau i} \int_l N_i N_j dy \int_\Omega \rho F_\tau F_s d\Omega \ddot{\mathbf{q}}_{sj} = \delta \mathbf{q}_{\tau i} \mathbf{M}^{ij\tau s} \ddot{\mathbf{q}}_{sj}
\tag{16}
$$

where $\mathbf{M}^{ij\tau s}$ is the fundamental nucleus of the element mass matrix and its components are written

in the following

$$M_{11}^{\tau sij} = M_{22}^{\tau sij} = M_{33}^{\tau sij} = \rho \int_l N_i N_j dy \int_\Omega F_\tau F_s d\Omega,$$

(17)

$$M_{12}^{\tau sij} = M_{13}^{\tau sij} = M_{21}^{\tau sij} = M_{23}^{\tau sij} = M_{31}^{\tau sij} = M_{32}^{\tau sij} = 0$$

In the case of static response analysis, the inertial contribution is neglected and the internal strain energy L_{int} is balanced by the work of external forces L_{ext}

$$\delta L_{\text{int}} = \delta L_{\text{ext}}$$

(18)

The external work of a generic point load **P**, for example, is given by

$$\delta L_{\text{ext}} = \delta \mathbf{u}^T \mathbf{P}$$

(19)

where

$$\mathbf{P} = \left\{ \begin{array}{ccc} P_x & P_y & P_z \end{array} \right\}^T$$

(20)

By introducing the shape functions and the generalized displacement approximation by CUF (see Eq. (10)), one has

$$\delta L_{\text{ext}} = F_\tau N_i \delta \mathbf{q}_{\tau i} \mathbf{P}$$

(21)

From Eq. (21), the variationally coherent fundamental nucleus of the loading vector which can be straightforwardly obtained. By using CUF, for a given expansion order, the fundamental nuclei can be expanded in an automatic manner to obtain the FE elemental arrays of the generic beam theory. For more details, the reader is referred to (Carrera *et al.* 2014).

4. Numerical results

The efficacy of the present 1D CUF beam model for structural analysis of different marine vessels is demonstrated. The beam cross section has been modelled using Lagrange Expansion (LE) functions whereby a $Component - Wise$ representation has been made for various structural features such as hull walls, the longitudinal stiffeners and the other stiffening elements. Therefore hereinafter, "CW" will refer to 1D CUF LE Beam model. Structural analyses of simplified models of container ship and boat structures have been presented in the following. The results from CUF beam formulation are compared with those from analytical and ANSYS 3D Solid model(hereinafter referred to as ANS3D). The strength of the CUF beam model in representing such complex geometries is well established over refined beam theories, since latter cannot accommodate such complexities. The CW model is more efficient over ANS3D models in terms of DoFs required to obtain the same level of accuracy.

4.1 Case-1: Container ship hull

A container ships may often find itself at an angle to the sea waves so that it is subjected to a torsional moment whose axis may assumed to be aligned to the ships's longitudinal axis. A typical container ship may be idealised in the form of a beam with C-type prismatic cross-section (Jensen

(a) Loading and constraints   (b) Deflected beam using CW Model
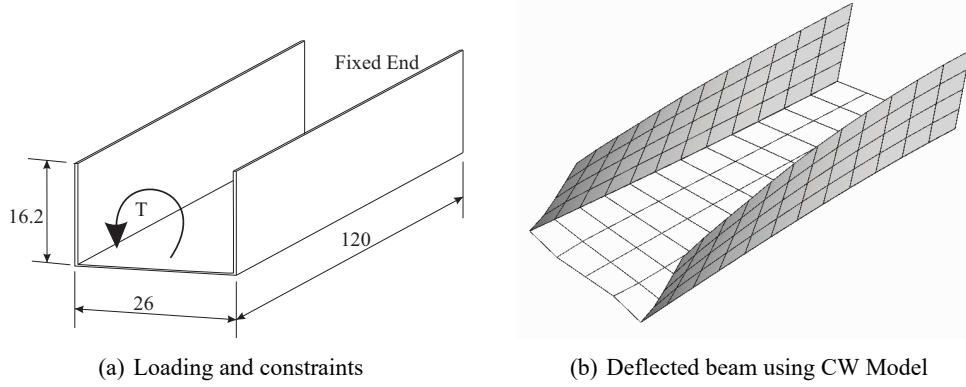
Fig. 3 Loading and constraints and deflection of a channel representation of a container ship (all dimensions in meters)

2001, Shama 2010). Because of this particular geometry, the ship has its shear center below the keel. Under a torsional loading, such structure exhibits not only the twist (pure rotation of cross section) but also an *out of plane* warping of the cross section. Moreover, if warping is restrained, there arise warping stresses, which are the stress components in the axial direction. Fig. 3(a) shows a channel representation of a container ship idealised as a beam subjected to an end torque $T = 2600000$ Nm. The other end of the beam is completely fixed. The beam has width $h = 26$ m, height $b = 16.2$ m, all wall thickness $t = 0.05$ m and length $l = 120$ m. The material is an alloy steel ($E = 210$ GPa, $\nu = 0.33$). This problem has been analysed analytically and numerically in order to demonstrate the capability of CW models to capture warping and associated stresses. Eq. (22) and Eq. (23) from (Budynas 2002) give, respectively, the torsional displacement at the loaded tip and the max deflection rate at the fixed end. The maximum warping stress, σ_w, emerges at the fixed end and it is obtained from Eq. (24), see (Shama 2010). The warping stress depends on the warping function ω, which is a parameter depending on the cross-section geometry. ω is obtained from the expressions provided in (Jensen 2001). For the channel section shown in Fig. 3(a), the warping function varies linearly over the wall height from the maximum value of $\omega = \dfrac{5}{8}b^2 = 5.23$ m^2 at the top and the minimum value of $\omega = -\dfrac{3}{8}b^2 = -3.14$ m^2 at the floor. The warping function varies anti-symmetrically over the floor width between $\omega = +\dfrac{3}{8}b^2$ and $\omega = -\dfrac{3}{8}b^2$. The torsional deflection and warping stress can be analytically found using Eq. (22) through Eq. (24). Various terms in the equations are explained in the following. These analytical relations employ assumption that the projection of the warped cross section remains unchanged while being rotated. The only displacement captured is axial deformation (or axial stresses for a constrained beam) while no in-plane kinematics for the cross section has been assumed

$$\theta_{\max} = \frac{T}{C_w E \beta^3}(\beta l - \tanh \beta l) \tag{22}$$

$$\theta''_{\max} = \frac{T}{C_w E \beta} \tanh \beta l \tag{23}$$

(a) Stress distribution in wall   (b) Stress distribution in floor
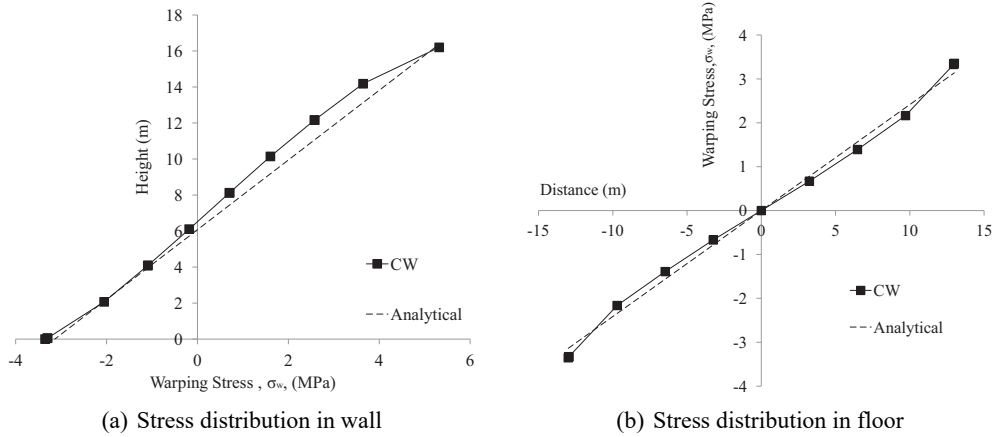
Fig. 4 CW and analytical warping stress plots

$$\sigma_w = \frac{\omega M}{C_w} \tag{24}$$

where

ω	:	Warping function			
M	:	Bi-moment acting over the cross section	$=$	$EC_w\theta''$	
C_w	:	Warping constant	$=$	$\dfrac{h^2b^3t}{12}\dfrac{2h+3b}{h+6b}$	$=$ 9778.4 m^6
J_t	:	Torsional constant	$=$	$\dfrac{t^3}{3}(h+2b)$	$=$ 0.00243 m^4
β	$=$	$\left[\dfrac{GJ_t}{EC_w}\right]^{1/2}$			$=$ 0.00031
E	:	Young's modulus			
G	:	Shear modulus			

The maximum torsional deflections obtained through the CW model and Eq. (22) were respectively 0.0429 and 0.0417 degrees. The warping stresses through CW and analytical solutions are plotted over the wall height and floor width in Fig. 4. The deformed configuration of the structure under consideration by CW model is also shown in Fig. 3(b). The CW model employed makes use of 13 B3 beam elements along the axis and a set of 14 L9 polynomials on the cross-section. The results clearly demonstrate the antisymmetric distribution of deflection and warping stress over the cross-section and CW values are fairly close to the analytical ones. Thus, the efficacy of employing CW models to analyse container ships is well established.

Having obtained sufficiently accurate results of a simplified container ship representation, a more realistic and detailed cross-section was modelled for a container ship. Fig. 5 shows the loading and geometry, which is a multi-cell double-walled construction. Owing to this open deck construction form, the shear center lies under the keel resulting in significant warping stresses under a torsional loading. The present model has the two ends fully constrained and the wave load is assumed to be distributed in triangular form. The distributed torque has the maximum value acting at mid-length.

(a) Triangular torque distribution   (b) Ship cross section
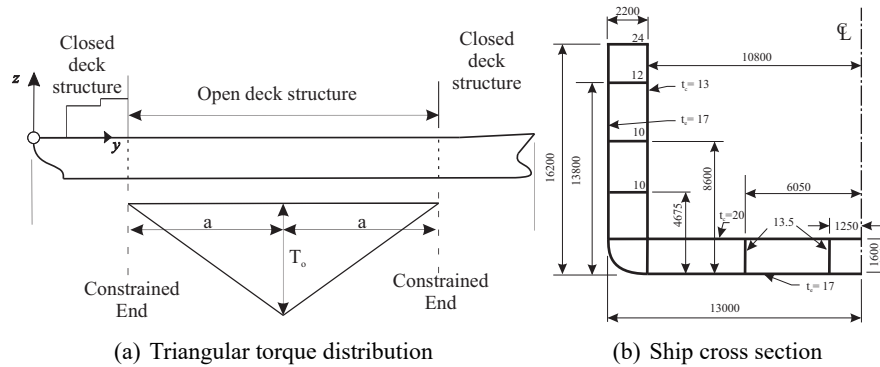
Fig. 5 Assumed torque distribution and cross section for a container ship (dimensions in mm)
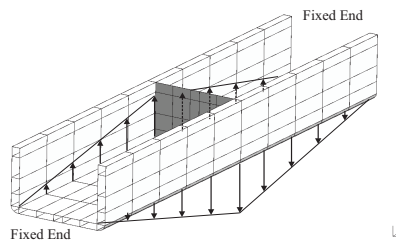
Fig. 6 CW model with loading and constraints

The configuration is analysed using the CW model and ANS3D model. In both the models, the torque is applied in the form of couple of forces applied along the two long inner edges. A bulk head at middle of the ship prevents severe in-plane displacements over the cross-section. The static analysis is aimed at obtaining warping stresses at the fixed ends and torsional displacement in the middle. The ship length is along y-axis while the cross section is symmetric about z-axis. The built-up structures at rear and fore ends provide fixed constraints and, thus, the flexible portion has a length equal to $2a$, which is the beam length under torsion. Total torque applied is 8100 ton$\times$m. The beam has length $2a = L = 120$ m, horizontal width equal to 26 m, height 16.2 m. The material is the same steel alloy as in the previous analysis case. Figure 6 shows the CW model with load vectors and the constraints applied. For ANS3D model, 130266 solid 185 brick element has been employed while in CW model, 11 Lagrange (B3) elements have used along the length. Regarding the CW model, 76 L9 polynomials have been employed to formulate the higher-order beam kinematics. As shown in Fig. 6, a reinforcement is assumed at the mid-span of the ship. This transverse reinforcement has the role to alleviate the differential bending in the plane of the cross-section and it is ideally modelled as a plane rigid structural element.

The results of the analysis are shown in Fig. 7 and Fig. 8. Figs. 7(a) and (b) show the torsional deflection of converged CW and ANS3D models, respectively. Fig. 8 shows the comparison of warping stress distribution over an inner edge near the constrained end for the CW model and ANS3D. The required DoFs for CW are 31473 while those for ANS3D are 762264. The results clearly demonstrate the accuracy of CW model in capturing the displacements requiring significantly less number

(a) CW, Max. displacement = 1.033 mm (DoFs = 31473)

(b) ANS3D, Max. displacement = 0.99 mm (DoFs = 762264)
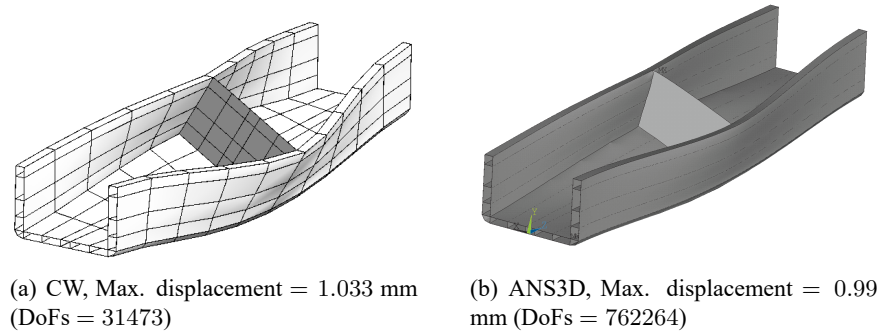
Fig. 7 Torsional deflections of CW and ANS3D models
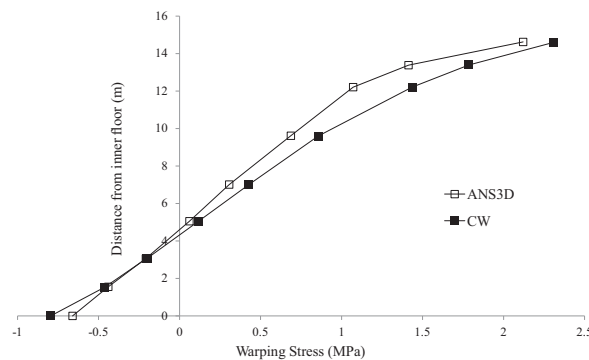
Fig. 8 Comparison of warping stress distribution over the inner vertical wall near constrained end

of DoFs. The warping stress distribution is fairly close to the results from ANS3D. The warping stresses result due to constraining the cross-section from warping freely.

4.2 Case-2: Boat structures

In previous section, the configuration involved structural components that were mutually orthogonal. The whole structure had a single beam axis aligned with y axis. Proceeding further towards a more realistic shape of a typical boat, the tapered or slanted flat faces are introduced in front and rear of the structure and the configurations are analysed using CW models with Lagrange polynomials above the cross-section. Each slanted wall is considered as a separate component modeled as a 1D beam with its own cross-section being the wall's thickness or its planar face. Thus, as a whole, the structure comprises of a network of various beams orientated at different angles. CUF, in fact, makes it possible to model very short beams (in the proposed example, the beam axis lays along the wall thickness, which is 10 mm) and large cross sections (e.g., the wall face is 2.12×0.56 m). The different components are connected at common nodes and their DoFs are shared. The idea of rotating refined CUF beam elements has been introduced by Carrera and Zappino (2016). Thus, it was possible to model a complex geometry as a network of various beams oriented at different angle.

Fig. 9 shows geometries being considered for structural analysis of boats with varying tapered configurations. The boat in Fig. 9(a) has taper inclined only to vertical plane, whereas the boat in

(a) Configuration-1: Boat with One-sided tapered Wall

(b) Configuration-2:Boat with Two-sided tapered Wall

(c) Configuration-3: Cabin added to the boat with two-sided taper
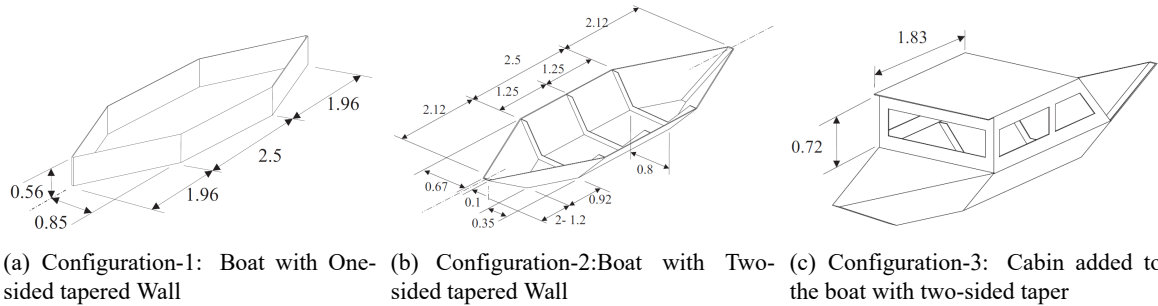
Fig. 9 Boat geometries with tapered walls incorporated in front and rear (all dimensions in meters, all wall thicknesses are 10 mm and ribs are 100 mm wide)

Fig. 9(b) has taper inclined to both the vertical and horizontal planes. The configuration shown in Fig. 9(c) has a cabin added to the former configurations. These structures cannot be modeled with typical beam theories and warrant the use of expensive 2D/3D solid elements. In this work, the proposed boat structures were modelled using CUF beams finite elements and the results were compared with those from ANSYS 3D solid elements. The modal analyses were performed for these structures followed by a static analysis for the boat configuration of Fig. 9(a).

4.2.1 Modal analyses

Modal analyses were performed for the configurations in Fig. 9 and the natural frequencies obtained through CW models are compared to ANS3D in Tables 1 and 2. Some selected mode shapes are shown in Fig. 10 and Fig. 11. These thin walled configurations require extensively heavy mesh when ANS3D solid elements are used, whereas the CW models required considerably less elements thereby less DoFs. The results clearly demonstrate that both the natural frequencies as well as the mode shapes from CUF beam model closely match those from ANSYS solid elements for most of the modes under consideration. It is seen that DoFs required by CUF beam are far less than the solid mesh of ANSYS for the same level of accuracy. It is also observed that employing a beam element of very small length and fairly large cross-section does not affect the accuracy of the proposed methodology. Also, the increase in the structural stiffness is evident through introduction of stiffeners and other features.

4.2.2 Static analysis

A static analysis was performed on the boat configuration of Fig. 9(a) as per loading and boundary conditions shown in Fig. 12. A point load of 1 kN is applied exactly at the mid point A on the upper surface of the bottom plate. Simply-supported boundary conditions are applied to the two edges on either sides of the boat. Deflections at point locations A and B from Fig. 12 are given in Table 3 along with the stresses at location A. The plot of the deformed configurations by the present beam model and ANSYS are shown in Fig. 13. The results demonstrate that with much less number of DoFs, CUF beam model captures the 3D kinematics of deflection and the stresses in close approximation to results from ANS3D model.

Table 1 Selected natural frequencies for the three boat configurations of Figs. 9(a)-(b)

(DOF)	CW (6777)	ANS3D (193425)	CW (12825)	ANS3D (217539)
	Configuration-1 Fig.9a		Configuration-2 Fig.9b	
Mode 1	7.522	7.433	15.831	14.937
Mode 2	10.498	10.835	20.126	18.434
Mode 3	13.462	13.485	25.478	25.130
Mode 4	14.527	14.608	28.022	28.201
Mode 5	22.020	23.420	28.276	28.866
Mode 6	24.286	24.390	32.072	33.230
Mode 7	27.857	25.331	32.899	34.315
Mode 8	29.087	26.696	37.542	38.260
Mode 9	29.436	32.591	41.307	39.019
Mode 10	30.105	33.967	43.371	44.954

Table 2 Selected natural frequencies for the boat Configuration-3 of Fig. 9(c)

(DOF)	CW (19125)	ANS3D (434130)
Mode 3	22.840	19.402
Mode 4	26.490	25.019
Mode 8	50.080	48.717
Mode 11	57.460	53.662

Table 3 Results under the loading shown in Fig. 12

Point	Model (DoFs)	Displacements (mm)	
		u	w
A	CW (6777)	0.000	-3.781
	ANS3D (193425)	0.000	-3.673
B	CW (6777)	1.754	-0.002
	ANS3D (193425)	1.732	-0.002
Point	Model (DoFs)	Stresses (MPa)		
		σ_{xx}	σ_{yy}	σ_{zz}
A	CW (6777)	7.72	9.57	0.619
	ANS3D (193425)	7.65	6.93	0.737

(a) Config-1, Mode-1: CW Model

(b) Config-1, Mode-1: ANS3D Model

(c) Config-1, Mode-2: CW Model

(d) Config-1, Mode-2: ANS3D Model

(e) Config-2, Mode-1: CW Model

(f) Config-2, Mode-1: ANS3D Model

(g) Config-2, Mode-2: CW Model

(h) Config-2, Mode-2: ANS3D Model
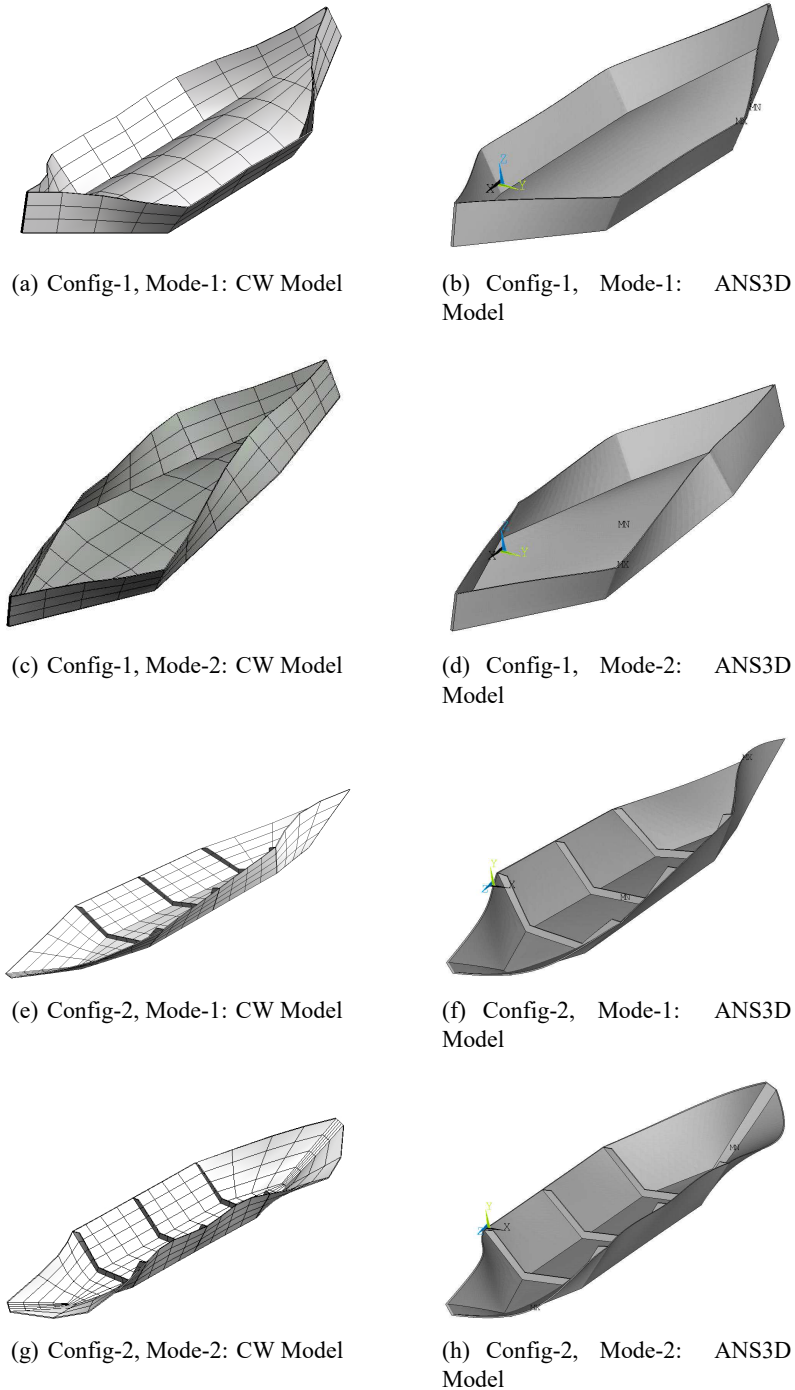
Fig. 10 First two deformed modes for each of the three configurations of Figs. 9(a)-(b)

(a) Config-3, Mode-3: CW Model

(b) Config-3, Mode-3: ANS3D Model

(c) Config-3, Mode-4: CW Model

(d) Config-3, Mode-4: ANS3D Model
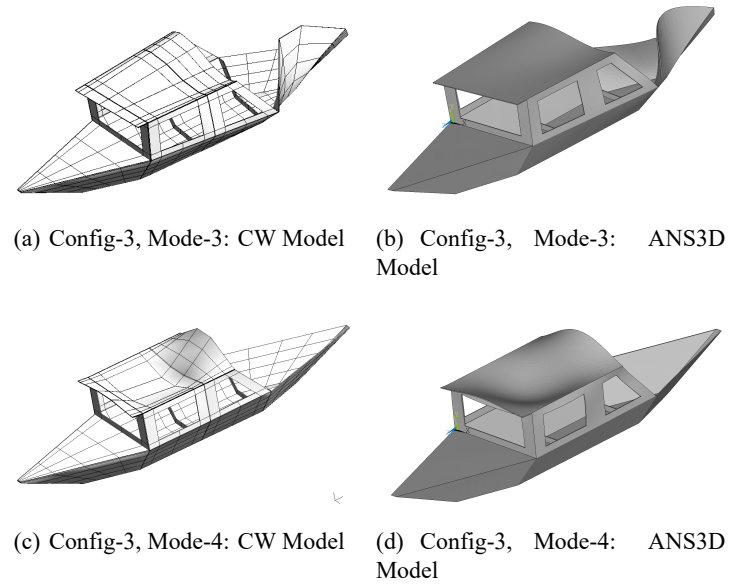
Fig. 11 Selected modes for the boat Configuration-3 of Fig. 9c
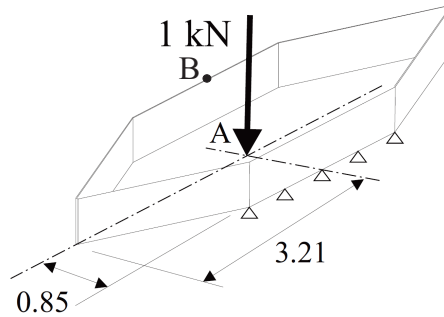
Fig. 12 Point load and boundary conditions for static analysis for boat geometry of Fig. 9(a) (all dimensions in meters and all wall thicknesses are 10 mm)

(a) Static Deflection from CW beam model

(b) Static Deflection from ANSYS 3D solid model
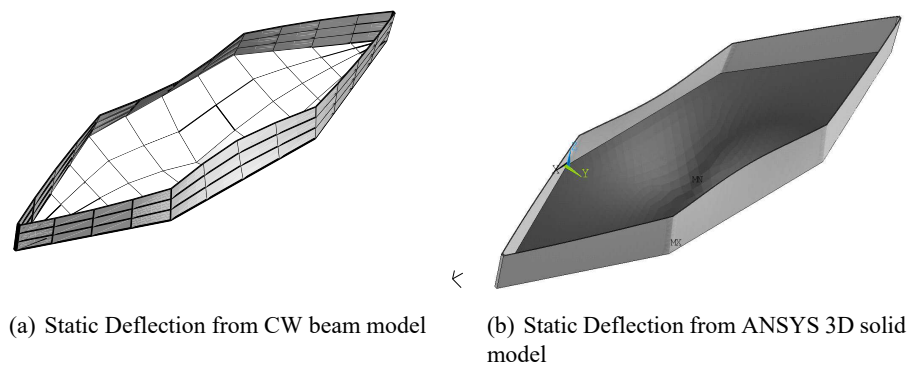
Fig. 13 Deflected boat under the loading shown in Fig. 12

5. Conclusions

In this paper, the Carrera Unified Formulation (CUF) was used for 1D finite element beam models and structural analyses of different marine vessels. The limitations of available refined beam theories were highlighted with regard to the cross-section warpage and in-plane displacements. Such aspects become important for marine vessels owing to their particular geometries. In various situations, the realistic and accurate results required use of commercial software which involved large DoFs, which renders the problem computationally heavy. It was demonstrated through results that both the said objectives are successfully achieved using CUF beam models. CUF can employ any class of expansion function to model cross-section kinematics. For present studies, Lagrange Expansion functions were used which manifested in an FEM model closest to a 3D Solid FEM model of a commercial software. These 1D models required far less (less than 1/10th) DoFs to obtain the results of ANSYS 3D solids for the same level of accuracy.

References

Bathe, K.J. (1996), *Finite Element Procedure*, Prentice Hall, New Jersey, USA.

Bishop, R.E.D. and Price, W.G. (1974), "On modal analysis of ship strength", *Proc. Roy. Soc. London A*, **341**(1624), 121-134.

Bishop, R.E.D. and Price, W.G. (1975), "Ship strength as a problem of structural dynamics", *The Naval Architect*, **2**, 61-63.

Bishop, R.E.D. and Price, W.G. (1979), *Hydroelasticity of Ships*, Cambridge University Press.

Budynas, W.C.Y.R.G. (2002), *Roark's Formulas for Stress and Strain*, McGraw-Hill.

Carrera, E., Cinefra, M., Petrolo, M. and Zappino, E. (2014), *Finite Element Analysis of Structures through Unified Formulation*, John Wiley & Sons.

Carrera, E. and Giunta, G. (2010), "Refined beam theories based on a unified formulation", *Int'l J. Appl. Mech.*, **2**(1), 117-143.

Carrera, E., Giunta, G., Nali, P. and Petrolo, M. (2010), "Refined beam elements with arbitrary cross-section geometries", *Comput. Struct.*, **88**(5-6), 283-293.

Carrera, E., Giunta, G. and Petrolo, M. (2011), *Beam Structures: Classical and Advanced Theories*, John Wiley & Sons. DOI: 10.1002/9781119978565.

Carrera, E. and Pagani, A. (2014), "Free vibration analysis of civil engineering structures by component-wise models", *J. Sound Vib.*, **333**(19), 4597-4620.

Carrera, E., Pagani, A. and Jamshed, J. (2016), "Refined beam finite elements for static and dynamic analysis of hull structures", *Comput. Struct.*, **167**, 37-49.

Carrera, E., Pagani, A. and Jamshed, R. (2015), "Refined beam finite element to analyse hull structures", *Proceedings of the International Conference on Lightweight Design of Marine Structures (LIMAS-2015)*, Glasgow, UK, November.

Carrera, E., Pagani, A. and Petrolo, M. (2013), "Classical, refined, and component-wise analysis of reinforced-shell wing structures", *AIAA J.*, **51**(5), 1255-1268.

Carrera, E., Pagani, A. and Petrolo, M. (2013), "Component-wise method applied to vibration of wing structures", *J. Appl. Mech.*, **80**(4), 1-15.

Carrera, E. and Petrolo, M. (2012), "Refined beam elements with only displacement variables and plate/shell capabilities", *Meccanica*, **47**(3), 537-556.

Carrera, E. and Zappino, E. (2016), "Carrera unified formulation for free-vibration analysis of aircraft structures", *AIAA J.*, **54**(1), 280-292.

Euler, L. (1744), *De curvis elasticis*, Lausanne and Geneva: Bousquet.

Jensen, J.J. (2001), *Load and Global Response of Ships*, Elsevier.

Jensen, J.J. and Madsen, H.F. (1977), "A review of ship hull vibration", *Shock Vib. Digest*, **9**(7).

Kawai, T. (1973), "The application of finite element methods to ship structures", *Comput. Struct.*, **3**(5), 117-594.

Leibowitz, R. (1961), "A method for prediction of slamming forces and response of a ship hull", *David Taylor Model Basin Report*, AD-428149.

Pedersen, P. (1983), "A beam model for the torsional-bending response of ship hulls", *Trans. Roy. Inst. Naval Arch.*, **125**, 171-182.

Pedersen, P. (1985), "Torsional response of container ships", *J. Ship Res.*, **29**, 194-205.

Pedersen, P. (1991), "Beam theories for torsional-bending response of ship hulls", *J. Ship Res.*, **35**(3), 254-265.

Pittaluga, A. (1978), "Recent developments in the theory of thin-walled beams", *Comput. Struct.*, **9**(1), 69-79.

Senjanovic, I. and Fann, Y. (1992), "A higher-order theory of thin-walled girders with application to ship structures", *Comput. Struct.*, **43**(1), 31-52.

Senjanovic, I. and Grubusic, R. (1991), "Coupled horizontal and torsional vibration of a ship hull with large hatch openings", *J. Ship Res.*, **41**(2), 213-226.

Shama, M. (2010), *Torsion and Stresses in Ships*, Springer.

Timoshenko, S. P. (1922a), "On the corrections for shear of the differential equation for transverse vibrations of prismatic bars", *Philosoph. Magazine*, **41**(245), 744-746.

Timoshenko, S.P. (1922b), "On the transverse vibrations of bars of uniform cross section", *Philosoph. Magazine*, **43**(253), 125-131.

Vlasov, V.Z. (1961), *Thin-walled elastic beams*, National Science Foundation, Washington.

EC